World Journal of Advanced Research and Reviews

eISSN: 2581-9615 CODEN (USA): WJARAI

Cross Ref DOI: 10.30574/wjarr

Journal homepage: https://wjarr.com/

(RESEARCH ARTICLE)

Check for updates

# Numerical Comparison of AT1 and AT2 gradient damage models within an incremental variational framework for coupled plasticity

Yan Zhang *

*Université de Lorraine, Nancy, France.*

World Journal of Advanced Research and Reviews, 2026, 31(02), 274–286

Publication history: Received on 27 June 2026; revised on 03 August 2026; accepted on 05 August 2026

Article DOI: https://doi.org/10.30574/wjarr.2026.31.2.2050

## Abstract

Gradient damage models are widely used to regularize strain localization and fracture in computational mechanics. Among the available formulations, the AT1 and AT2 models differ primarily in the adopted crack-density function, leading to distinct damage initiation and evolution characteristics. Although both formulations have been extensively studied for brittle fracture, their responses under identical constitutive assumptions within a unified incremental variational framework remain of considerable interest. In this work, the AT1 and AT2 gradient damage models are compared numerically within an incremental variational framework for gradient damage coupled with perfect plasticity. The formulation is implemented using the finite element method, where the displacement field, plastic internal variables, and damage field are determined within a unified incremental variational framework using an alternating minimization procedure. Both models are evaluated using identical material parameters, loading conditions, and numerical discretization to ensure a consistent comparison. Numerical simulations of a displacement-controlled tensile benchmark are performed to examine damage evolution, plastic strain localization, and energy dissipation. The results show that the AT2 formulation predicts earlier damage initiation, wider damage localization, and higher local plastic strain, whereas the AT1 formulation delays localization and accumulates greater damage-weighted plastic dissipation. The present study provides a consistent assessment of the influence of the crack-density function on coupled damage–plasticity behaviour and contributes to a better understanding of the characteristics of the AT1 and AT2 formulations.

**Keywords:** Gradient damage; Incremental variational formulation; Perfect plasticity; Finite element method; FEniCS

## 1. Introduction

Engineering materials often undergo both irreversible plastic deformation and progressive damage during mechanical loading, making their mechanical response highly nonlinear. Plastic deformation accounts for the irreversible strains accumulated after yielding, whereas damage progressively reduces the effective stiffness of the material, leading to strain localization and ultimately fracture. Lemaitre [1] first established the framework of continuum damage mechanics to describe the progressive degradation of materials. This framework was subsequently extended by Lemaitre and Chaboche [2], who developed constitutive theories coupling damage with plasticity and highlighted the strong interaction between these two irreversible mechanisms. Accurately capturing this interaction is therefore essential for predicting the nonlinear response and failure of engineering materials. Since then, coupled damage–plasticity modelling has become an active area of research in computational mechanics. A comprehensive treatment of computational inelastic constitutive modelling can be found in the monograph by Simo and Hughes [3].

Conventional continuum damage models are generally formulated in a local setting, in which the damage state at a material point depends only on the variables evaluated at that point. Although such models can describe stiffness

* Corresponding author: Yan Zhang

degradation and material softening, their finite element implementation may suffer from pathological strain localization and strong mesh dependence once the material enters the softening regime. The origin of this difficulty was analysed by Bažant [4], who showed that conventional local softening continua may lead to ill-posed responses and localization into an arbitrarily small region. To regularize this behaviour, Peerlings et al. [5] introduced a gradient-enhanced damage formulation in which an internal length scale controls the width of the localization zone. A closely related development emerged from the variational theory of brittle fracture proposed by Francfort and Marigo [6], where crack initiation and propagation are governed by the minimization of a global energy functional. Bourdin et al. [7] subsequently introduced a regularized approximation that replaces the sharp crack by a continuous damage field, making the variational formulation suitable for numerical computation. Its finite element implementation and alternating minimization solution strategy were further analyzed by Bourdin [8]. This regularized variational approach was later developed into widely used phase-field and gradient-damage formulations, including the thermodynamically consistent framework of Miehe et al. [9] and the general class of gradient damage models studied by Pham et al. [10]. These developments have led to several regularized gradient damage formulations, among which the AT1 and AT2 models are the two most widely adopted approaches.

Despite sharing the same variational foundation, the AT1 and AT2 formulations exhibit distinct regularization characteristics. Both approximate sharp cracks by means of a continuous damage field, but their principal difference lies in the crack-density function, which is linear in AT1 and quadratic in AT2. This apparently simple modelling choice leads to different damage initiation and evolution characteristics: AT1 generally exhibits an initial elastic stage associated with a finite damage threshold, whereas AT2 allows a more gradual development of damage from the early stages of loading. The energetic consequences of different crack-density functions were systematically investigated by Pham et al. [10], while Tanné et al. [11] further examined their influence on crack nucleation and the prediction of critical loading conditions. A broader theoretical interpretation of these regularization choices was subsequently provided by Wu [12] within a unified phase-field framework for damage and quasi-brittle failure. These inherent differences suggest that the choice between AT1 and AT2 may influence not only damage evolution and localization but also the overall mechanical response when damage is coupled with plasticity. A comparison of the two formulations under identical constitutive assumptions, loading conditions, and numerical settings is therefore valuable for clarifying their respective characteristics and applicability in coupled damage–plasticity analyses.

The distinct regularization characteristics of the AT1 and AT2 formulations motivate a systematic investigation of how the choice of damage model influences the coupled damage–plasticity response when all other modelling ingredients remain unchanged. Addressing this question requires a numerical framework that enables a consistent and objective comparison between different damage formulations. A variational formulation of constitutive updates was first introduced by Ortiz and Stainier [13], who demonstrated that incremental constitutive evolution can be derived from a minimum principle. This variational viewpoint was subsequently generalized to dissipative solids by Yang et al. [14] and further developed for gradient plasticity within a unified energetic framework by Nguyen [15]. Such an incremental variational framework provides a consistent basis for coupled damage–plasticity simulations because the displacement field and internal variables are determined within a unified incremental variational framework without requiring separate local constitutive updates. Within this unified framework, the influence of the damage regularization itself can be assessed consistently by maintaining identical constitutive assumptions, material parameters, boundary conditions, loading histories, and numerical discretization while changing only the gradient damage formulation.

In this work, a unified incremental variational finite element implementation is employed to investigate the coupled response of gradient damage and perfect plasticity. The AT1 and AT2 formulations are incorporated under identical constitutive assumptions, material parameters, loading conditions, and numerical discretization to ensure a consistent basis for comparison. Representative numerical examples are presented to examine their influence on the global mechanical response, damage evolution, plastic strain development, and localization behaviour. The results provide a consistent assessment of the influence of damage regularization on coupled damage–plasticity simulations and contribute to a better understanding of the respective characteristics of the AT1 and AT2 formulations.

## 2. Incremental Variational Framework

This section presents the constitutive ingredients required for the incremental variational formulation adopted in this work. The kinematic assumptions are first introduced, followed by the Helmholtz free energy, the plastic dissipation, and the gradient damage regularization. These ingredients are then combined to formulate the incremental minimization problem, after which the corresponding finite element implementation is presented.

## 2.1. Constitutive formulation

The constitutive model is formulated under the assumptions of infinitesimal strains, quasi-static loading, and rate-independent material behaviour. Under the small-strain setting, the infinitesimal strain tensor is defined as:

$$\boldsymbol{\varepsilon} = \nabla^{s}\boldsymbol{u} = \frac{1}{2}(\nabla\boldsymbol{u} + (\nabla\boldsymbol{u})^{T}), \tag{1}$$

where $\boldsymbol{u}$ denotes the displacement field. The total strain is additively decomposed into elastic and plastic parts,

$$\boldsymbol{\varepsilon} = \boldsymbol{\varepsilon}^{e} + \boldsymbol{\varepsilon}^{p}, \qquad \boldsymbol{\varepsilon}^{e} = \boldsymbol{\varepsilon} - \boldsymbol{\varepsilon}^{p}, \tag{2}$$

which provides the kinematic basis for the constitutive formulation developed below.

### 2.1.1. Helmholtz free energy

The reversible constitutive response is characterized by the Helmholtz free energy density. A scalar damage variable $\alpha$ is introduced to represent material degradation, where $\alpha = 0$ corresponds to the undamaged state and $\alpha = 1$ denotes complete failure. The Helmholtz free energy density is defined as:

$$\psi(\boldsymbol{\varepsilon}, \boldsymbol{\varepsilon}^{p}, \alpha) = g(\alpha)\psi_{0}^{e}(\boldsymbol{\varepsilon} - \boldsymbol{\varepsilon}^{p}). \tag{3}$$

Material degradation is described by the quadratic degradation function:

$$g(\alpha) = (1-\alpha)^{2} + k, \tag{4}$$

where $k \ll 1$ is a small residual stiffness parameter introduced to prevent the stiffness matrix from becoming singular in fully damaged regions.

The elastic energy density of the undamaged material is given by:

$$\psi_{0}^{e}(\boldsymbol{\varepsilon}^{e}) = \frac{1}{2}\boldsymbol{\varepsilon}^{e} : \mathbf{C}_{0} : \boldsymbol{\varepsilon}^{e}, \tag{5}$$

where $\mathbf{C}_{0}$ denotes the fourth-order elasticity tensor of the undamaged material. For isotropic linear elasticity, this expression becomes

$$\psi_{0}^{e}(\boldsymbol{\varepsilon}^{e}) = \mu\boldsymbol{\varepsilon}^{e} : \boldsymbol{\varepsilon}^{e} + \frac{\lambda}{2}[\mathrm{tr}(\boldsymbol{\varepsilon}^{e})]^{2}, \tag{6}$$

where $\lambda$ and $\mu$ are the Lamé parameters.

The corresponding Cauchy stress is obtained by differentiating the free-energy density with respect to the total strain,

$$\boldsymbol{\sigma} = \frac{\partial\psi}{\partial\boldsymbol{\varepsilon}} = g(\alpha)\mathbf{C}_{0} : (\boldsymbol{\varepsilon} - \boldsymbol{\varepsilon}^{p}). \tag{7}$$

### 2.1.2. Rate-independent plastic dissipation

The irreversible plastic response is described using a classical rate-independent $J_2$ von Mises perfect plasticity model with yield stress $\sigma_0$. Under the assumption of plastic incompressibility, the plastic strain rate satisfies

$$\mathrm{tr}(\dot{\boldsymbol{\varepsilon}}^{p}) = 0. \tag{8}$$

The rate of accumulated equivalent plastic strain is defined as

$$\dot{p} = \sqrt{\frac{2}{3}}|\dot{\boldsymbol{\varepsilon}}^{p}|, \tag{9}$$

where $|\cdot|$ denotes the Euclidean norm of a second-order tensor.

Within the variational formulation, the plastic evolution is governed by the rate-independent dissipation potential

$$\phi^{p}(\dot{\boldsymbol{\varepsilon}}^{p}, \dot{p}; \alpha) = b(\alpha)\sigma_{0}\dot{p} + I_{\mathcal{K}}(\dot{\boldsymbol{\varepsilon}}^{p}, \dot{p}), \tag{10}$$

where $b(\alpha) = (1-\alpha)^2$ is the degradation function for the plastic dissipation, and $I_{\mathcal{K}}$ denotes the indicator function of the admissible set $\mathcal{K}$. The admissible set is defined as

$$\mathcal{K} = \left\{ (\dot{\boldsymbol{\varepsilon}}^p, \dot{p}) \,\middle|\, \mathrm{tr}(\dot{\boldsymbol{\varepsilon}}^p) = 0, \quad \dot{p} \geq \sqrt{\frac{2}{3}} |\dot{\boldsymbol{\varepsilon}}^p| \right\}. \tag{11}$$

The indicator function is given by

$$I\_\mathcal{K}(\dot{\boldsymbol{\varepsilon}}^{\mathrm{p}}, \dot{p}) = \begin{cases} 0, & \text{if } (\dot{\boldsymbol{\varepsilon}}^p, \dot{p}) \in \mathcal{K} \\ +\infty, & \text{otherwise} \end{cases}. \tag{12}$$

This formulation incorporates plastic incompressibility and the equivalent-plastic-strain constraint directly into the variational problem. For an active plastic evolution, the inequality in Eq. 11 is attained as an equality.

*2.1.3. Gradient damage dissipation*

To regularize damage localization and avoid pathological mesh dependence, the damage evolution is described through the gradient damage contribution

$$\phi^d(\alpha, \nabla\alpha) = \frac{G_c}{c_w}\left[\frac{w(\alpha)}{l_c} + l_c|\nabla\alpha|^2\right], \tag{13}$$

where $G_c$ is the fracture toughness, $l_c$ is the internal length parameter controlling the width of the regularized damage zone, $w(\alpha)$ is the crack-density function, and $c_w$ is the associated normalization constant defined as

$$c_w = 4\int_0^1 \sqrt{w(s)}\mathrm{d}s. \tag{14}$$

The AT1 and AT2 gradient damage models differ in the choice of the crack-density function. For the AT1 model,

$$w_{\mathrm{AT1}}(\alpha) = \alpha, \qquad c_w^{\mathrm{AT1}} = \frac{8}{3}. \tag{15}$$

whereas the AT2 model is defined by

$$w_{\mathrm{AT2}}(\alpha) = \alpha^2, \qquad c_w^{\mathrm{AT2}} = 2. \tag{16}$$

The linear crack-density function employed in the AT1 model introduces a finite threshold for damage initiation, whereas the quadratic function of the AT2 model permits damage to develop progressively from the early stages of loading. Damage irreversibility is enforced through the constraint $\alpha_n \leq \alpha_{n+1}$ , which is incorporated into the incremental variational formulation presented in Section 2.2.

For the numerical comparison presented in this work, the same elastic degradation function, plasticity model, material parameters, boundary conditions, and numerical discretization are used for both formulations. Therefore, the crack-density function $w(\alpha)$and its associated normalization constant $c_w$ constitute the principal distinction between the AT1 and AT2 models.

## 2.2. Incremental variational formulation

The loading process is discretized into a sequence of pseudo-time steps

$$0 = t_0 < t_1 < \cdots < t_N = T. \tag{17}$$

Here, the pseudo-time parameter is introduced solely to describe the successive loading states and does not represent physical time, consistent with the rate-independent character of the constitutive model. At load step $t_n$, the state variables $(\boldsymbol{u}, \boldsymbol{\varepsilon}^p, p, \alpha)$ are assumed to be known. The increments of the plastic strain and the accumulated equivalent plastic strain are then defined as

$$\Delta\boldsymbol{\varepsilon}^p = \boldsymbol{\varepsilon}^p - \boldsymbol{\varepsilon}_n^p, \qquad \Delta p = p - p_n. \tag{18}$$

Based on the constitutive ingredients introduced above, the material response at each loading step is characterized by an incremental potential comprising the elastic stored energy, the rate-independent plastic dissipation, the gradient damage contribution, and the external work.

At load step $n+1$, the incremental potential is written as

$$\Pi_{n+1}(\boldsymbol{u}, \boldsymbol{\varepsilon}^p, p, \alpha) = \tag{19}$$

$$\int_{\Omega} [\psi(\boldsymbol{\varepsilon}(\boldsymbol{u}), \boldsymbol{\varepsilon}^p, \alpha) + \phi^p(\Delta\boldsymbol{\varepsilon}^p, \Delta p; \alpha) + \phi^d(\alpha, \nabla\alpha)] \, d\Omega - W_{\text{ext},n+1}(\boldsymbol{u}).$$

Here, $W_{\text{ext},n+1}$ denotes the external work at load step $n+1$. In the numerical examples considered below, loading is imposed through prescribed boundary displacements, while body forces and prescribed boundary tractions are neglected.

The updated state at load step $n+1$ is obtained by solving the incremental minimization problem

$$\left(\boldsymbol{u}_{n+1}, \boldsymbol{\varepsilon}^p_{n+1}, p_{n+1}, \alpha_{n+1}\right) = \arg\min \Pi_{n+1} \left(\boldsymbol{u}, \boldsymbol{\varepsilon}^p, p, \alpha\right), \tag{20}$$

subject to the prescribed displacement boundary conditions and the damage admissibility constraint

$$\alpha_n \leq \alpha \leq 1. \tag{21}$$

The lower bound enforces damage irreversibility, whereas the upper bound restricts the damage variable to its physically admissible range. Plastic incompressibility and the equivalent-plastic-strain constraint are enforced through the indicator function contained in the dissipation potential $\phi^p$.

The displacement field, the plastic internal variables, and the damage field are therefore determined within a unified incremental variational framework, without requiring a separate local return-mapping procedure. The numerical strategy adopted to solve the resulting coupled minimization problem is presented in the following subsection.

### 2.3. Numerical implementation

The incremental variational problem is spatially discretized using the finite element method. The computational domain $\Omega$ is partitioned into a conforming mesh $\mathcal{T}_h$. The displacement field $\boldsymbol{u}$ is approximated using vector-valued first-order continuous Galerkin elements (CG1), while the damage variable $\alpha$ is discretized using scalar CG1 elements. The plastic strain $\boldsymbol{\varepsilon}^p$ is represented in Voigt notation using vector-valued first-order discontinuous Galerkin elements (DG1), and the accumulated plastic strain $p$ is approximated using scalar DG1 elements. The discontinuous approximation allows the plastic internal variables to evolve element-wise without imposing interelement continuity. Following spatial discretization, the incremental variational problem is reduced to a finite-dimensional optimization problem.

The coupled elastoplastic-damage problem is solved using an alternating minimization procedure. At each loading step, the elastoplastic subproblem is first solved while keeping the damage field fixed:

$$\left(\boldsymbol{u}^{(k+1)}, \boldsymbol{\varepsilon}^{p,(k+1)}, p^{(k+1)}\right) = \arg\min \Pi^{\text{ep}}_{n+1} \left(\boldsymbol{u}, \boldsymbol{\varepsilon}^p, p; \alpha^{(k)}\right), \tag{22}$$

where $\Pi^{\text{ep}}_{\text{n+1}}$ comprises the degraded elastic energy and the rate-independent plastic dissipation. The prescribed displacement boundary conditions are imposed directly through the admissible displacement space, while plastic incompressibility and the equivalent-plastic-strain constraint are enforced through the indicator function introduced in Section 2.1.2.

The updated displacement and plastic internal variables are then held fixed, and the damage subproblem is solved according to

$$\widetilde{\alpha^{(k+1)}} = \arg\min \Pi^{\text{d}}_{n+1} \left(\alpha; \boldsymbol{u}^{(k+1)}, \boldsymbol{\varepsilon}^{p,(k+1)}, p^{(k+1)}\right), \tag{23}$$

where $\Pi^{\text{d}}_{\text{n+1}}$ contains the degraded elastic contribution and the gradient damage regularization. After each damage solve, the computed damage field is projected onto the interval $0 \leq \alpha \leq 1$. Damage irreversibility is subsequently enforced pointwise by preventing the damage variable from decreasing relative to the damage field at the beginning of the current loading step.

The elastoplastic and damage subproblems are alternately solved until both the total energy and the damage field satisfy the prescribed convergence criteria. Once convergence is reached, the history variables are updated and the computation proceeds to the next loading increment.

The complete solution procedure is summarized in Fig. 1.

The formulation is implemented in the FEniCS finite element framework [16, 17], while the convex optimization problems are formulated using the fenics_optim package [18] and solved with the MOSEK optimization solver [19]. The same mesh, finite element spaces, loading increments, convergence criteria, and solver settings are used for the AT1 and AT2 simulations. Therefore, the differences between the two sets of results arise from the selected crack-density function and its associated normalization constant.

**Input:** Finite element mesh, material parameters, boundary conditions, loading increments, maximum alternate iterations $N_{\mathrm{alt}}$, and tolerances $\mathrm{tol}_E$ and $\mathrm{tol}_\alpha$

**Output:** Converged fields $\{\boldsymbol{u}, \boldsymbol{\varepsilon}^p, p, \alpha\}$ and associated energies at each loading step

Initialize $\boldsymbol{\varepsilon}^{p,0}$, $p^0$, and $\alpha^0$;

**for** $i = 1, \ldots, N_{\mathrm{inc}}$ **do**

Apply the prescribed loading at increment $i$;

Set the history fields from the previous converged state:

$$\boldsymbol{\varepsilon}^{p,\mathrm{hist}} \leftarrow \boldsymbol{\varepsilon}^{p,i-1}, \qquad p^{\mathrm{hist}} \leftarrow p^{i-1}, \qquad \alpha^{\mathrm{hist}} \leftarrow \alpha^{i-1}.$$

Initialize the trial fields from the history state and evaluate the initial total energy $E^0$;

**for** $k = 1, \ldots, N_{\mathrm{alt}}$ **do**

Store the previous damage field $\alpha^{i,k-1}$ and energy $E^{k-1}$;

**Elastoplastic subproblem:**;

Solve for fixed $\alpha^{i,k-1}$:

$$\left(\boldsymbol{u}^{i,k}, \boldsymbol{\varepsilon}^{p,i,k}, p^{i,k}\right) = \underset{\boldsymbol{u},\boldsymbol{\varepsilon}^p,p}{\arg\min}\, \Pi^{\mathrm{ep}}\left(\boldsymbol{u}, \boldsymbol{\varepsilon}^p, p; \alpha^{i,k-1}\right).$$

**Damage subproblem:**;

Solve for fixed $\left(\boldsymbol{u}^{i,k}, \boldsymbol{\varepsilon}^{p,i,k}, p^{i,k}\right)$:

$$\widetilde{\alpha}^{i,k} = \underset{0\le\alpha\le 1}{\arg\min}\, \Pi^{\mathrm{d}}\left(\alpha; \boldsymbol{u}^{i,k}, \boldsymbol{\varepsilon}^{p,i,k}, p^{i,k}\right).$$

Enforce damage irreversibility:

$$\alpha^{i,k} \leftarrow \max\left(\widetilde{\alpha}^{i,k}, \alpha^{\mathrm{hist}}\right).$$

**Convergence check:**;

Compute the total energy $E^k$ and the relative variations:

$$r_E^k = \frac{\left|E^k - E^{k-1}\right|}{\max\left(1, \left|E^k\right|, \left|E^{k-1}\right|\right)},$$

$$r_\alpha^k = \frac{\left\|\alpha^{i,k} - \alpha^{i,k-1}\right\|_2}{\max\left(1, \left\|\alpha^{i,k-1}\right\|_2\right)}.$$

**if** $r_E^k < \mathrm{tol}_E$ *and* $r_\alpha^k < \mathrm{tol}_\alpha$ **then**

break;

Accept the converged solution at loading step $i$;

Compute and store the elastic, plastic, damage, and total energies;

Output the converged fields and associated energies;

**Figure 1** Alternating minimization algorithm for coupled elasto-plasticity and gradient damage.

## 3. Results and Discussion

This section compares the responses predicted by the AT1 and AT2 gradient damage models for a rectangular specimen subjected to displacement-controlled tensile loading. The comparison focuses on the spatial evolution of damage and plastic deformation and on the associated energy evolution. Identical geometric, material, loading, and numerical settings are adopted for both models so that the observed differences can be attributed directly to the selected crack-density function.

### 3.1. Benchmark configuration and material parameters

A two-dimensional rectangular specimen subjected to displacement-controlled tensile loading is considered as the benchmark problem. The geometry, dimensions, and boundary conditions are illustrated in Fig. 2. Plane strain conditions are assumed throughout the analysis. A prescribed horizontal displacement ū is applied on the right boundary, whereas the horizontal displacement is constrained on the left boundary.

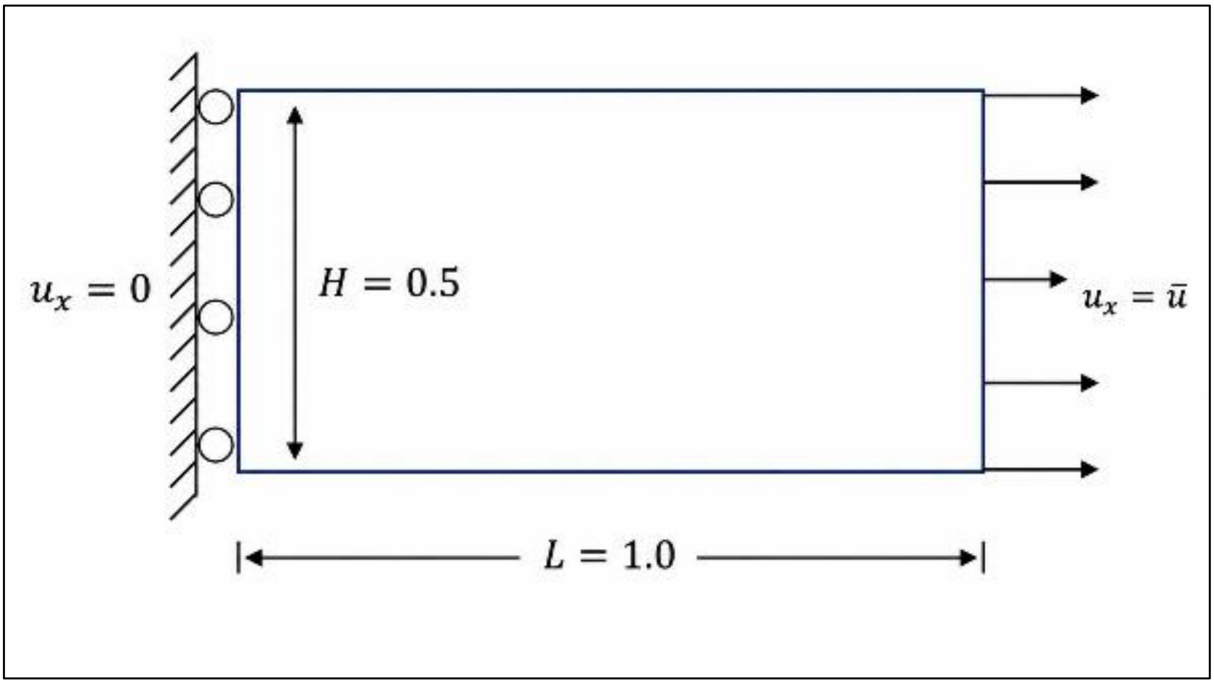


**Figure 2** Geometry of the rectangular specimen.

The material is modeled using isotropic linear elasticity coupled with von Mises perfect plasticity and gradient damage. The material parameters adopted in the simulations are summarized in Table 1. The numerical study is conducted in a normalized, dimensionless setting; therefore, all geometric, material, loading, and energy quantities are reported in a consistent dimensionless form. This normalization does not affect the comparison between the AT1 and AT2 formulations because the same parameter values and numerical settings are employed in both cases.

Unless otherwise stated, the same geometry, material properties, loading history, mesh discretization, convergence tolerances, and solver settings are used for both models.

**Table 1** Normalized material parameters used in the numerical simulations.

| Parameter | Symbol | Value |
|---|---|---|
| Young's modulus | $E$ | 1.00 |
| Poisson's ratio | $\nu$ | 0.30 |
| Yield stress | $\sigma_0$ | 1.00 |
| Fracture toughness | $G_c$ | 1.78 |
| Internal length | $l_c$ | 0.10 |
| Residual stiffness | $k$ | $10^{-6}$ |

### 3.2. Comparison of damage evolution

Fig. 3 compares the evolution of the damage field predicted by the AT1 and AT2 models at four loading stages. Both formulations eventually produce an inclined damage band extending across the specimen. Nevertheless, clear differences are observed in the onset and subsequent development of damage.

The AT2 model exhibits damage at an earlier loading stage. At $u_x = 6$, a distinct inclined damaged zone has already developed in the AT2 simulation, whereas the AT1 specimen remains essentially undamaged. At $u_x = 12$, a weak localization band becomes visible in the AT1 result, while the corresponding AT2 band is already strongly developed. This delayed response is consistent with the finite damage-initiation threshold associated with the linear crack-density function of the AT1 model. By contrast, the quadratic crack-density function of the AT2 model allows damage to evolve progressively without such a finite threshold.

With increasing prescribed displacement, the localization bands predicted by both formulations become more pronounced. In the AT1 model, the damage field develops gradually from a narrow and initially weak band into a well-defined localized zone. The AT2 model, however, maintains a broader damaged region, with a more diffuse transition from the highly damaged core to the surrounding undamaged material. At the later loading stages, $u_x = 18$ and $u_x = 24$, both models predict a continuous inclined band with damage levels approaching unity along its center, although the AT2 band remains spatially wider. These results demonstrate that the crack-density function governs not only the onset of damage but also the subsequent width and intensity of the localized zone. Relative to AT1, the AT2 formulation predicts an earlier onset of damage, a wider damaged region, and a more strongly developed central localization band. Since damage evolution is coupled with plastic deformation, the corresponding development of the accumulated plastic strain is examined in the following subsection.

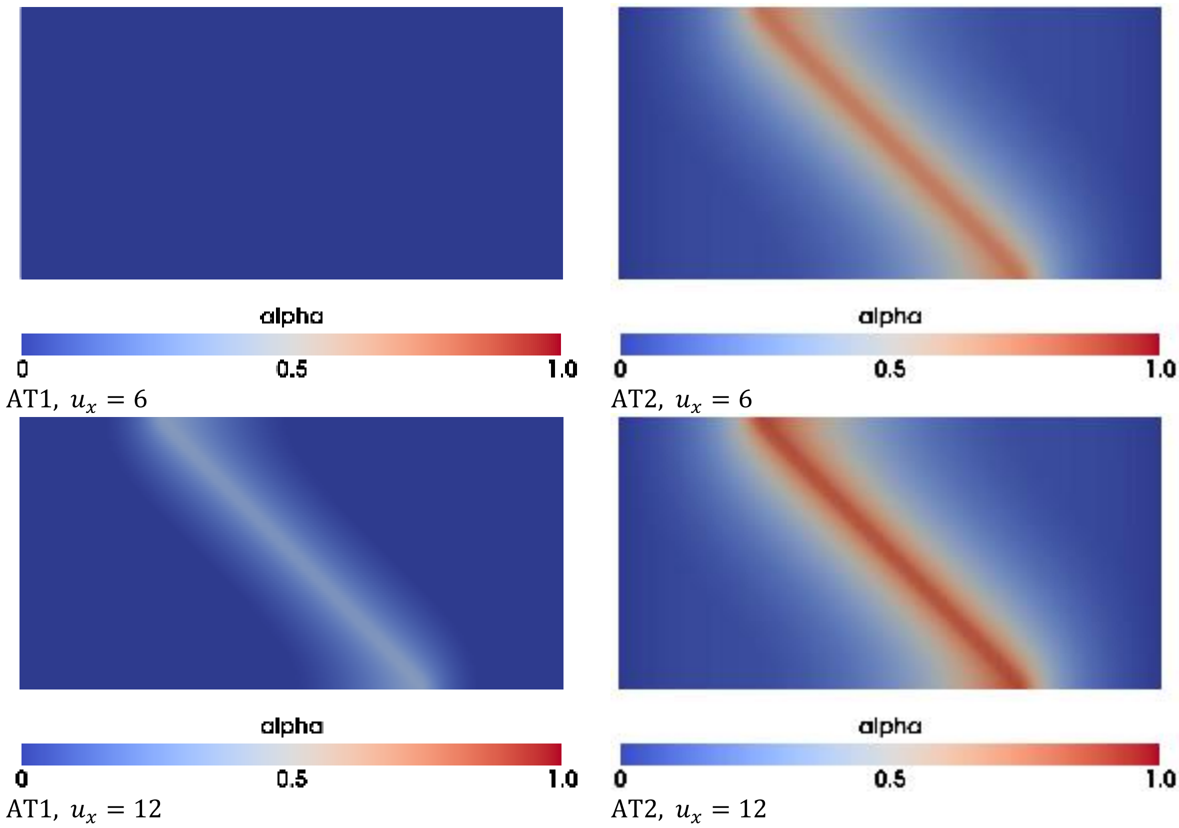

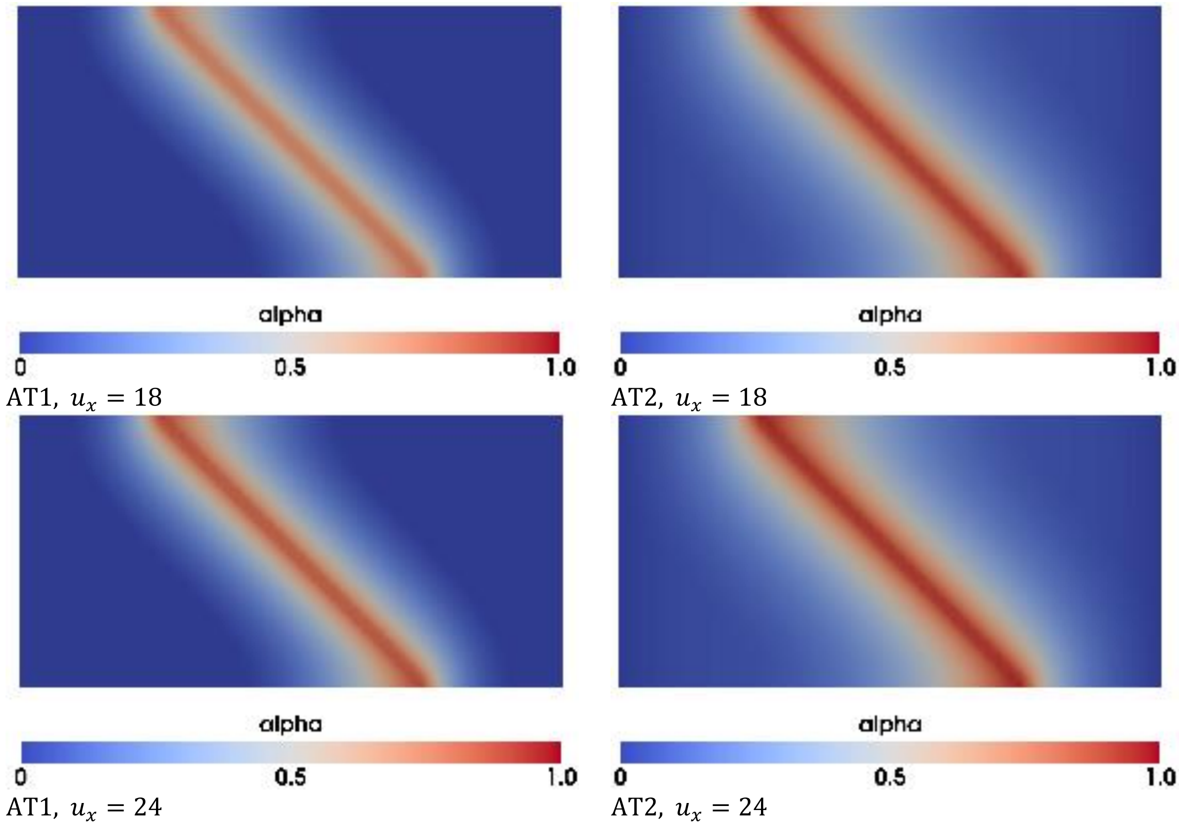


**Figure 3** Evolution of the damage variable $\boldsymbol{\alpha}$ for the AT1 (left column) and AT2 (right column) models at prescribed displacement levels ($\boldsymbol{u_x = 6, 12, 18, 24}$).

### 3.3. Comparison of plastic strain evolution

Fig. 4 compares the evolution of the plastic strain magnitude predicted by the AT1 and AT2 models at the same four prescribed displacement levels. The plotted quantity corresponds to the magnitude of the plastic strain represented in Voigt form. Different color scales are used for the two formulations because substantially different ranges are obtained. The color intensity must therefore be interpreted with reference to the color bar associated with each column and should not be compared directly between the AT1 and AT2 results.

Consistent with the damage distributions shown in Fig. 3, the AT2 model exhibits plastic localization at an earlier loading stage. At $u_x = 6$, a distinct inclined plastic zone is already visible in the AT2 specimen, whereas the plastic strain magnitude remains negligible in the AT1 simulation. In the AT1 model, a clearly localized plastic band develops only at a later loading stage.

For both formulations, plastic deformation is concentrated along the same inclined path as the corresponding damage band. This close spatial correspondence reflects the strong coupling between damage localization and irreversible plastic deformation. In contrast to the relatively broad transition regions observed in the damage fields, the plastic response is confined to a narrow band located near the core of the damaged zone.

As the prescribed displacement increases, the magnitude of the localized plastic strain increases in both models, while the orientation and spatial position of the band remain essentially unchanged. The ranges indicated by the corresponding color bars show that the AT2 formulation produces larger plastic strain magnitudes at the considered loading stages. This behavior is consistent with the earlier development of plastic localization in the AT2 model, which allows irreversible deformation to accumulate over a larger portion of the loading history.

These results demonstrate that the choice of crack-density function influences not only damage initiation and localization but also the onset and intensity of the associated plastic response. Relative to AT1, the AT2 formulation predicts earlier plastic localization and larger plastic strain magnitudes under the same prescribed displacement levels.

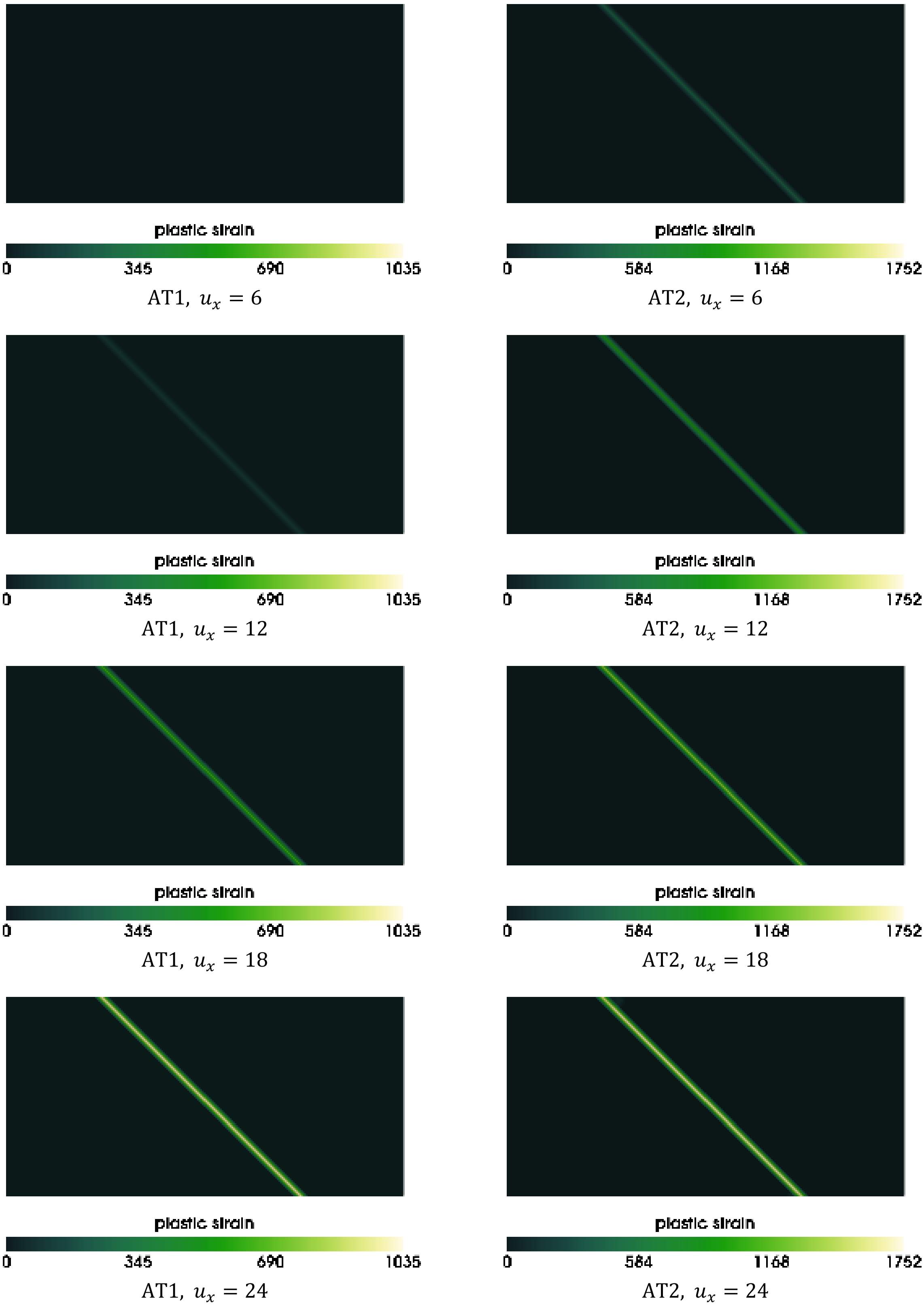


**Figure 4** Evolution of the plastic strain magnitude predicted by the AT1 model (left column) and the AT2 model (right column) at prescribed displacement levels ($\boldsymbol{u_x} = \mathbf{6}, \mathbf{12}, \mathbf{18}, \mathbf{24}$). Different color scales are used for the two models.

### 3.4. Comparison of energy evolution

To clarify the energetic quantities reported below, the elastic, damage, and accumulated plastic contributions at loading step *n* are evaluated as

$$E_{\mathrm{el}}^{n} = \int_{\Omega} g(\alpha_n)\psi_0^e\big(\boldsymbol{\varepsilon}(\boldsymbol{u}_n) - \boldsymbol{\varepsilon}_n^p\big)d\Omega, \tag{24}$$

$$E_{\mathrm{d}}^{n} = \int_{\Omega} \frac{G_c}{c_w}\left[\frac{w(\alpha_n)}{l_c} + l_c|\nabla\alpha_n|^2\right]d\Omega, \tag{25}$$

$$E_{\mathrm{p}}^{n} = \sum_{j=1}^{n}\int_{\Omega} b\big(\alpha_{j-1}\big)\sigma_0\,\Delta p_j d\Omega, \tag{26}$$

where $b(\alpha)$ is the plastic-dissipation degradation function introduced in Section 2.1.2. The total energy is defined as

$$E_{\mathrm{tot}}^{n} = E_{\mathrm{el}}^{n} + E_{\mathrm{d}}^{n} + E_{\mathrm{p}}^{n}. \tag{27}$$

Fig. 5 compares the evolution of the elastic, damage, accumulated plastic, and total energies for the AT1 and AT2 formulations. Different vertical scales are used in the two panels because the AT1 model produces substantially larger energy values. Consequently, quantitative comparisons should be based on the axis values rather than on the apparent curve heights.

In both models, the elastic energy increases during the initial loading stage and subsequently decreases as damage develops and the effective stiffness is degraded. However, the timing of this transition differs markedly. In the AT2 model, the elastic energy reaches its maximum at a very early loading stage and rapidly approaches zero. In contrast, the AT1 model retains a finite elastic contribution over a considerably longer loading interval before it decreases sharply following damage initiation. The damage and accumulated plastic energies increase monotonically in both cases, while the total energy gradually approaches a plateau.

The most pronounced difference between the two formulations concerns the accumulated plastic contribution. Although the AT2 model exhibits earlier plastic localization and larger local plastic strain magnitudes, its global accumulated plastic energy remains substantially lower than that of the AT1 model. This behavior can be explained by the degradation function $b(\alpha)$ appearing in the plastic dissipation. Because damage develops early in the AT2 model, a considerable portion of the subsequent plastic deformation occurs in regions where $b(\alpha)$ has already been strongly reduced. The corresponding plastic increments therefore make a limited contribution to the global damage-weighted plastic dissipation.

By contrast, the delayed damage initiation predicted by the AT1 model allows plastic deformation to accumulate over a longer loading interval while $b(\alpha)$ remains relatively close to unity. This results in a markedly larger accumulated plastic energy and, consequently, a higher total energy. The AT1 model also produces a larger damage-energy contribution at the later loading stages, although the difference in plastic energy constitutes the dominant contribution to the separation between the two total-energy curves.

The energy evolution is therefore consistent with the field distributions presented in Fig. 3 and Fig. 4. The AT2 formulation promotes earlier damage and plastic localization, whereas the AT1 formulation delays damage initiation and accumulates a larger damage-weighted plastic dissipation before severe stiffness degradation occurs. These results demonstrate that the crack-density function influences not only the local development of damage and plastic deformation but also the global energetic response of the coupled system.

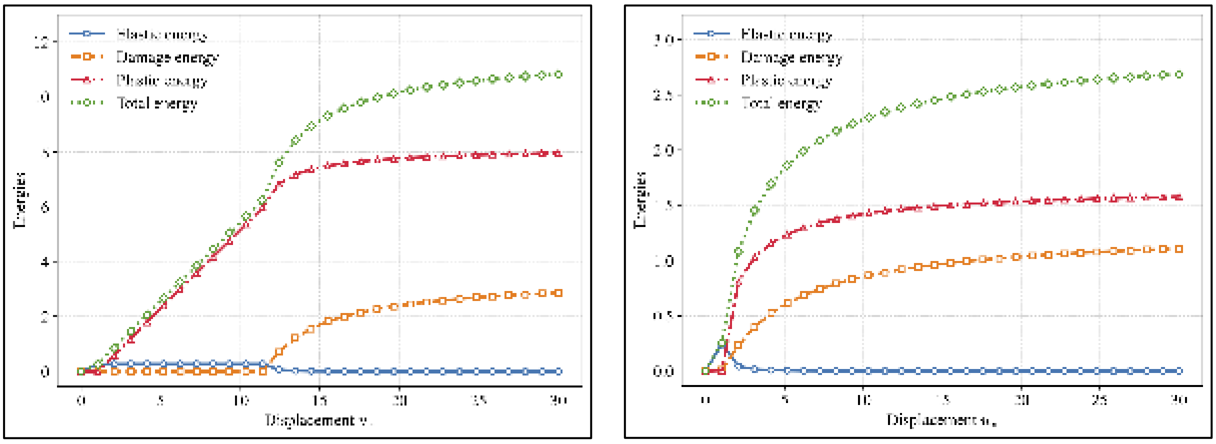


(a) Energy evolution for AT1 model

(b) Energy evolution for AT2 model

**Figure 5** Comparison of the energy evolution for the (a) AT1 and (b) AT2 models. Different vertical scales are used in the two panels.

## 4. Conclusion

This paper compared the responses of the AT1 and AT2 crack-density formulations within a unified incremental variational framework for gradient damage coupled with von Mises perfect plasticity. A rectangular tensile benchmark was used to examine the evolution of damage, plastic strain, and the associated energy contributions under identical numerical and material settings.

The numerical results revealed clear differences between the two formulations. Compared with AT1, the AT2 model predicted an earlier onset of damage and an earlier development of plastic localization. It also produced a broader damaged region and larger local plastic strain magnitudes. By contrast, the AT1 formulation exhibited a delayed and comparatively sharper localization process.

The energy results further showed that larger local plastic strain does not necessarily lead to larger accumulated plastic dissipation. In the present formulation, the plastic dissipation is weighted by the damage-dependent degradation function. Consequently, plastic increments occurring in highly damaged regions contribute less to the accumulated plastic energy. This mechanism explains why the AT2 model developed stronger local plastic deformation while exhibiting lower plastic and total energy levels than the AT1 model.

Overall, the results demonstrate that the choice of crack-density function influences not only the onset and spatial development of damage, but also its interaction with plastic deformation and the resulting global energetic response. Neither formulation can be regarded as universally superior on the basis of the present benchmark. Instead, the AT1 and AT2 models produce distinct coupled responses within the same incremental variational framework. Future work may extend the present comparison to strain-hardening plasticity, more complex loading conditions, and additional geometrical configurations.

## Compliance with ethical standards

### *Disclosure of conflict of interest*

The author declares that there are no conflicts of interest.

### *Statement of ethical approval*

This study did not involve human participants, animals, or personal data; therefore, ethical approval and informed consent were not required.

## References

[1] Lemaitre J. A continuous damage mechanics model for ductile fracture. J Eng Mater Technol. 1985;107(1):83-89.

[2] Lemaitre J, Chaboche JL. Mechanics of solid materials. Cambridge: Cambridge University Press; 1990.

[3] Simo JC, Hughes TJR. Computational inelasticity. New York: Springer; 1998.

[4] Bažant ZP, Belytschko TB. Wave propagation in a strain-softening bar: Exact solution. J Eng Mech. 1985;111(3):381-389.

[5] Peerlings RHJ, de Borst R, Brekelmans WAM, de Vree JHP. Gradient enhanced damage for quasi-brittle materials. Int J Numer Methods Eng. 1996;39(19):3391-3403.

[6] Francfort GA, Marigo JJ. Revisiting brittle fracture as an energy minimization problem. J Mech Phys Solids. 1998;46(8):1319-1342.

[7] Bourdin B, Francfort GA, Marigo JJ. Numerical experiments in revisited brittle fracture. J Mech Phys Solids. 2000;48(4):797-826.

[8] Bourdin B. Numerical implementation of the variational formulation for quasi-static brittle fracture. Interfaces Free Bound. 2007;9(3):411-430.

[9] Miehe C, Welschinger F, Hofacker M. Thermodynamically consistent phase-field models of fracture: Variational principles and multi-field finite element implementations. Int J Numer Methods Eng. 2010;83(10):1273-1311.

[10] Pham K, Amor H, Marigo JJ, Maurini C. Gradient damage models and their use to approximate brittle fracture. Int J Damage Mech. 2011;20(4):618-652.

[11] Tanné E, Li T, Bourdin B, Marigo JJ, Maurini C. Crack nucleation in variational phase-field models of brittle fracture. J Mech Phys Solids. 2018;110:80-99.

[12] Wu JY. A unified phase-field theory for the mechanics of damage and quasi-brittle failure. J Mech Phys Solids. 2017;103:72-99.

[13] Ortiz M, Stainier L. The variational formulation of viscoplastic constitutive updates. Comput Methods Appl Mech Eng. 1999;171(3-4):419-444.

[14] Yang Q, Stainier L, Ortiz M. A variational formulation of the coupled thermo-mechanical boundary-value problem for general dissipative solids. J Mech Phys Solids. 2006;54(2):401-424.

[15] Nguyen QS. Quasi-static responses and variational principles in gradient plasticity. J Mech Phys Solids. 2016;97:156-167.

[16] Logg A, Mardal KA, Wells GN, editors. Automated solution of differential equations by the finite element method: The FEniCS book. Berlin: Springer; 2012.

[17] Alnæs MS, Blechta J, Hake J, Johansson A, Kehlet B, Logg A, et al. The FEniCS Project version 1.5. Arch Numer Softw. 2015;3(100):9-23.

[18] Bleyer J. fenics_optim-Convex optimization interface in FEniCS. Zenodo. 2020.

[19] MOSEK ApS. MOSEK Optimization Toolbox for Python manual. Version 11.0. Copenhagen: MOSEK ApS; 2025. Available from: https://docs.mosek.com/11.0/pythonapi/index.html.